Research Article

A single nonsynonymous mutation on ZIKV E protein-coding sequences leads to markedly increased neurovirulence *in vivo*

Zhihua Liu [a,b,c,1], Yawei Zhang [d,1], Mengli Cheng [d,1], Ningning Ge [a,b,c], Jiayi Shu [c], Zhiheng Xu [e], Xiao Su [a,b], Zhihua Kou [c,*], Yigang Tong [f,***], Chengfeng Qin [d,**], Xia Jin [c,*]

[a] *Institut Pasteur of Shanghai, Chinese Academy of Sciences, Shanghai, 200031, China*
[b] *University of Chinese Academy of Sciences, Beijing, 100049, China*
[c] *Vaccine and Immunology Research Center, Translational Medical Research Institute, Shanghai Public Health Clinical Center, Fudan University, Shanghai, 201508, China*
[d] *State Key Laboratory of Pathogen and Biosecurity, Beijing Institute of Microbiology and Epidemiology, Beijing, 100071, China*
[e] *State Key Laboratory of Molecular Developmental Biology, CAS Center for Excellence in Brain Science and Intelligence Technology, Institute of Genetics and Developmental Biology, Chinese Academy of Sciences, Beijing, 100101, China*
[f] *College of Life Science and Technology, Beijing University of Chemical Technology, Beijing, 100029, China*

ARTICLE INFO

ABSTRACT

Zika virus (ZIKV) can infect a wide range of tissues including the developmental brain of human fetus. Whether specific viral genetic variants are linked to neuropathology is incompletely understood. To address this, we have intracranially serially passaged a clinical ZIKV isolate (SW01) in neonatal mice and discovered variants that exhibit markedly increased virulence and neurotropism. Deep sequencing analysis combining with molecular virology studies revealed that a single 67D (Aspartic acid) to N (Asparagine) substitution on E protein is sufficient to confer the increased virulence and neurotropism *in vivo*. Notably, virus clones with D67N mutation had higher viral production and caused more severe cytopathic effect (CPE) in human neural astrocytes U251 cells *in vitro*, indicating its potential neurological toxicity to human brain. These findings revealed that a single mutation D67N on ZIKV envelope may lead to severe neuro lesion that may help to explain the neurovirulence of ZIKV and suggest monitoring the occurrence of this mutation during nature infection may be important.

1. Introduction

Zika virus (ZIKV) infection received worldwide attention when it triggers a global pandemic during 2015–2016. The virus was first isolated in the ZIKA forest of Uganda in 1947, causing only a handful of documented self-liming mild febrile illness during a period of sixty years, and thus it had long been neglected until the occurrence of ZIKV endemics in Yap Island in 2007 (Duffy et al., 2009) and French Polynesia in 2013 (Cao-Lormeau et al., 2014; Jouannic et al., 2016), and epidemics in Americas since 2014 (Pierson et al., 2018). These recent large outbreaks afflicted an accumulative millions of people and revealed some previously unappreciated facts that ZIKV infection is strongly associated with increased incidences of microcephaly in newborns, Guillain-Barré syndrome in adults, and persistent infection in male genital tissues (Baud et al., 2017). Among these severe complications, the link between congenital ZIKV infection and birth defect in infants has made the strongest psychological impact on the public (Driggers et al., 2016; Li et al., 2016; Miner et al., 2016; Mlakar et al., 2016; Nielsen-Saines et al., 2019; Yockey et al., 2016).

The long quiescent period followed by sudden major ZIKV outbreaks maybe resulted from several factors including viral sequence mutations, increased competence of mosquito vector, and widely available susceptible populations (Musso et al., 2019). The interaction between ZIKV and its host has been an area of intensive study more recently, some of which revealed the influences of viral genetics. An evolutionary Alanine to Valine (A188V) mutation on the nonstructural protein 1 (NS1) increases

---

* Corresponding authors. Vaccine and Immunology Research Center, Translational Medical Research Institute, Shanghai Public Health Clinical Center, Fudan University, Shanghai, 201508, China.
** Corresponding author. State Key Laboratory of Pathogen and Biosecurity, Beijing Institute of Microbiology and Epidemiology, Beijing, 100071, China.
*** Corresponding author. College of Life Science and Technology, Beijing University of Chemical Technology, Beijing, 100029, China.
E-mail addresses: kouzhihua@shphc.org.cn (Z. Kou), tong.yigang@gmail.com (Y. Tong), qincf@bmi.ac.cn (C. Qin), jinxia@shphc.org.cn (X. Jin).
[1] These authors contributed equally to this work.

ZIKV infectivity in mosquitoes and also helps the virus to evade interferon induction in murine cells *in vitro* and experimentally infected mice *in vivo* (Liu et al., 2017; Xia et al., 2018). A Serine to Asparagine (S139N) mutation on the pre-membrane (prM) protein of viral strains isolated between 2013 and 2014 has an increased neurovirulence (Yuan et al., 2017). By functional comparison between ZIKV strains, however, it was found that the contemporary Asian strains responsible for the recent outbreaks (and linked to microcephaly) have neither more infectivity to neuronal cells *in vitro* (Simonin et al., 2016), nor more neurovirulence *in vivo*, than the older African strains (Shao et al., 2017; Udenze et al., 2019), leaving the specific virological cause of neurological diseases during the current pandemics remain unanswered.

Other studies have placed more emphasis on the global interactions between virus and host. A worse disease outcome has been associated with high levels of virus RNA persisting in human fetal and neonatal central nervous system (CNS) *in vivo* (Bhatnagar et al., 2017; Brito et al., 2018), possibly through infection of neuronal cells, as demonstrated by experimental infection of fetal neurocytes *in vitro* (Hanners et al., 2016). Preexisting *anti*-flavivirus immunity can also worsen clinical outcomes, through antibody dependent enhancement (ADE) of ZIKV infectivity, as demonstrated in murine models (Bardina et al., 2017; Brown et al., 2019; Rathore et al., 2019), and non-human primate models (Robbiani et al., 2019). Overall, the existing literature concurs with the idea that ZIKV infection can lead to disorders in fetal and neonatal central nervous system but differs on the specific virus genetic features that cause such disease outcomes.

To study these questions on pathogenesis, various animal models have been developed, most of which use immunodeficient mice susceptible to ZIKV infection such as A129 (129 background, lacking IFN-α/β receptor), AG129 (129 background, lacking both IFN-α/β and IFN-γ receptors), A6 (C57BL/6 background, lacking IFN-α/β receptor), AG6 (C57BL/6 background, lacking both IFN-α/β and IFN-γ receptors); Signal transducer and activator of transcription 2 (Stat2) deficient mice, and Recombination activating gene 1 (Rag1) deficient mice (Dowall et al., 2016; Gorman et al., 2018; Lazear et al., 2016; Liu et al., 2017; Rossi et al., 2016). ZIKV can also infect wild type neonatal mice and cause diseases that resemble to some extent microcephaly, paralysis, and seizure (Li et al., 2018; Manangeeswaran et al., 2016; Nem de Oliveira Souza et al., 2018). Mechanistically, these neurological manifestations have been linked to infection of neuron progenitor cells and other neurocytes (Li et al., 2016; Shao et al., 2017; Zhang et al., 2017). Of note, comparative analysis between human and rodents has shown that mouse brain at postnatal day 1–2 roughly corresponds to the human fetal brain at mid-gestation stage (Auvin et al., 2013, Semple et al., 2013). Therefore, newborn mice have also been used as a model for studying the influence of ZIKV infection on CNS development.

Combining traditional and novel animal models and viral genetic analyses, here we report the isolation and characterization of ZIKV variants accumulated during sequential *in vivo* passage of a clinical isolate SZ-WIV01 (SW01) in neonatal mice. Significantly, a viral variant with a single nonsynonymous nucleotide mutation on position 1069 of ZIKV open reading frame (G1069A), corresponding to an amino acid change (D67N) on the E protein, is sufficient to account for 100–1000-fold increase in its neurovirulence. These data provide experimental evidence in support of the idea that viral genetic evolution alters ZIKV disease manifestations and offers a plausible explanation of the recent observed association between ZIKV infection and the increased incidence of neurological disorders.

2. Materials and methods

2.1. Mouse experiments

BALB/c and C57BL/6 mice were purchased (Vital River Laboratory Animal Technology Co., Ltd, Beijing) and bred under specific pathogen free (SPF) conditions at the BSL2 Animal Core facility (A-BSL-2) at Institut Pasteur of Shanghai. BALB/c and C57BL/6 pregnant mice were housed separately before being delivered to the BSL-2 laboratory. DP2 (2 days post-delivery) and DP7 (7 days post-delivery) offspring mice were infected with indicated ZIKV strain through subcutaneous (s.c.) or intracranial (i.c.) injection. Body weight, survival rate and clinical score were monitored daily according to experimental design.

2.2. Cell lines and viruses

Vero-E6, BHK-21 and human astrocytes U251 cells were grown at 37°C in Dulbecco's Modified Eagle Medium (DMEM) (Gibco, USA) supplemented with 10% fetal bovine serum (FBS) (Gibco, USA) and 1% penicillin and streptomycin (P/S). Mosquito C6/36 cells were cultured in Modified Eagle Medium (MEM) (Gibco, USA) with 10% FBS, 1% P/S and 1% non-essential amino acids (NEAA). ZIKV clinical isolate SW01 (also known as SZ-WIV01, GenBank: MH055376.1) was kindly provided by Wuhan Institute of Virology, Chinese Academy of Sciences. SW01 was propagated once in C6/36 cells with MEM (Gibco) plus 2% FBS, 1% P/S and 1% non-essential amino acids. Rescued viral mutants with the backbone of ZIKV CAM-2010 infectious clone was passaged once in C6/36 cells. All amplified viruses were aliquoted into 2 mL vials and stocked at −80°C until use.

2.3. Virus titration

Virus titer was determined by titration on Vero-E6 monolayer. Briefly, Vero-E6 cells were seeded on 24 well plates (1.2×10^5 cells/well) one day prior to infection, and washed once next day with DMEM without FBS. Virus was 10-fold serially diluted, then added at 200 μL/well to the Vero cell monolayer, followed by incubation at 37°C for 2 h. The supernatant containing virus was replaced by 1.2 mL DMEM with 1.5% FBS, 1% CMC (carboxymethylcellulose), then incubated at 37°C, 5% CO_2 for 96 h. Four days later, the overlay was removed, and cells were fixed with 4% PFA for 30 min. The viral plaque was visualized by staining with 0.25% crystal violet, and then counted.

2.4. Adaptation of SW01 in vivo

ZIKV clinical isolate SW01 (10^3 PFU/10 μL) was injected into the brain λ point of DP2 neonatal BALB/c mice. At the indicated time (1–12 days and 8 days) post infection, mice were anaesthetized, and brains were collected and homogenized in 1 mL sterile PBS, and then centrifuged to collect supernatant, which was aliquoted for viral titration and storage at −80°C. A new round of *in vivo* infection into the mouse brain was performed after viral titration.

2.5. Determination of virus burden in tissues

At the indicated time (3-, 6- and 11-days post infection), ZIKV infected mice were euthanized, and their tissues were collected, fixed with Trizol (Invitrogen, USA) reagent. RNA was extracted according to the manufactures' manual, then aliquoted and stored at −80°C before use. RNA concentration was determined by Nanodrop (2000) (Thermo fisher, USA). Reverse transcription with ZIKV specific primer (Rev-AAGTGATCCATGT-GATCAGTTGATCC) was performed using FastQuant RT Kit (Tiangen). Real-time PCR was done on 7900HT (ABI) machine using Fast Fire qPCR Premix (Probe) (Tiangen). Virus RNA copies were calculated with a standard curve. The primers are as follows: (For: CAACCACAGCAAGCGGAAG, Rev: AAGTGATCCATGTGATCAGTTGATCC, Probe: 5'-FAM/TGGTATG-GAATGGA GATAAGGC/MGB-3').

2.6. Immunostaining of brain sections

Dissected brains were immediately immersed in 4% paraformaldehyde (PFA) and fixed for 24 h, and then embedded into paraffin, followed by being sectioned into 4 μm slices using Leica RM2016. After

being deparaffinized with xylene and ethanol, rehydrated with ethanol and H$_2$O, sections were blocked in blocking buffer (3% BSA-PBS) for 30 min, then incubated with primary antibody to ZIKV E protein (1:1000 diluted in blocking buffer) (cat.no: BF-1176-56; BioFront) overnight at 4°C. On day 2, the sections were incubated in fluorescence labelled secondary antibody (1:400 dilution) (GB25301, Servicebio) at RT for 1 h. Nucleus were stained with DAPI (G1012, Servicebio) at RT for 10 min. Original images were captured and visualized using a Nikon Eclipse C1 Ortho-Fluorescent microscope with Nikon DS-U3 image system. All immunofluorescent images were analyzed with the Pannoramic Viewer (3DHISTECH), ImageJ, and GraphPad V8 software.

2.7. Single clone selection and E protein sequencing

Stocks of SW01 and MA-SW01 virus were serially diluted and seeded on Vero monolayer in 24 well plates. Four days post infection, the supernatants from wells containing single virus plaque were collected and amplified in C6/36 cells once, and viral titer was determined by standard plaque assay. For E protein sequencing, RNA of single virus clone was extracted by Viral RNA Mini Kit (QIAGEN) and reversely transcribed using PrimeScript™ II 1st Strand cDNA Synthesis Kit (Takara) with virus envelope protein gene specific primer (Env-Rev primer: CGGGGATCCC-GAGCAGAGACGGCTGTGGATAAG). Virus *E* gene was amplified by PCR (Env-For primer: CGAAGCTTATGATCAGGTGCATAGGAGTCAGCA, Env-Rev primer: CGGGGATCCCGAGCAGAGACGGCTGTGGATAAG), then cloned into pEASY-Blunt Cloning Kit (Transgen) and sequenced by Sanger method.

2.8. Next generation sequencing (NGS) of ZIKV

Virus stocks were filtered through a 0.45 µm filter before nucleic acid extraction. Virus RNA was extracted from 400 µL of filtered supernatant with the High Pure Viral RNA Kit (Roche). The sequencing library was constructed using Ion Total RNA-Seq Kit v2 (Thermo Fisher Scientific) and sequenced on an Ion S5 sequencer (Thermo Fisher Scientific). Low quality reads and short reads were excluded, the remaining reads were assembled by mapping to the reference sequence MH055376 using CLC Genomic Workbench (ver 9.0). The mutation site was manually checked with the original sequencing data. iSNV and Graphing were performed on CLCGenomic Workbench and Origin. NGS raw data were available at Sequence Read Archive (SRA) of NCBI (Access number: SRP237251).

2.9. Generation of ZIKV infectious clone containing mutations

An infectious cDNA clone (pFLZIKV) containing the full-length genome of CAM-2010 strain of ZIKV (CAM-WT) were used as the backbone for introducing specific nucleotides substitutions into envelope protein (D67N, M68I) or NS2A protein (A117T), singly or combined, using the Q5 site directed mutagenesis kit (NEB). All these mutations were then confirmed by DNA sequencing. The full-length infectious clones were rescued as described previously (Shan et al., 2016).

2.10. Indirect immunofluorescence assay (IFA)

Viral RNA was transfected into BHK-21 cells using Lipofectamine 3000 reagent (Thermo Fisher Scientific) according to the manufacturer's instructions. At 24, 48, and 72 h post infection, the infected cells were fixed in acetone/methanol (V/V = 3/7) at −20 °C for 15 min, and then used for detection of ZIKV E protein expression by IFA as described previously (Liu et al., 2016).

2.11. Virus growth kinetics in multiple cell lines

Briefly, U251, Vero, A549 and C636 cells were seeded on 24 well plates (1×10^5 cells/well) one day prior to infection, and washed once next day with DMEM (for U251, Vero, A549) or MEM (for C636) without FBS. Cells were infected with wild type virus CAM-WT or mutant virus CM1-A (E protein D67N mutant) at multiplicity of infection (MOI) of 0.1. Two or four days later, morphology and pathology of mock treated or ZIKV infected cells were recorded by camera. Virus titers of supernatant from ZIKV infected cells at indicated time were titrated on Vero monolayers.

2.12. Statistical analysis

Survival curves were analyzed by log-rank test. All summary data were compared using either student's *t*-test or two-way ANOVA. All analyses were performed on Graphpad Prism V8.0 platform. Statistical significance levels were reported as the following: "*" for $P < 0.05$; "**" for $P < 0.01$; "***" for $P < 0.001$.

3. Results

3.1. In vivo adaptation of a ZIKV clinical isolate SW01 in neonatal mice gives rise to variants with increased virulence

ZIKV SW01 (SZ-WIV01 strain) is a clinical isolate recovered in 2016 from a Chinese patient returned from an epidemic region, Samoa (Deng et al., 2016). The virus was propagated twice on C6/36 cells. To discover the potential variant causing severe neuropathy, we serially passaged ZIKV SW01 through a classical *in vivo* adaptation model, in which 2 days post-neonatal (DP2) BALB/c mice were injected with 1000 PFU of virus by intracranial (i.c.) route (Fig. 1A). Brains of infected mice were collected from days 2–12 post infection, minced, filtered, and then used for measuring virus titer with standard plaque assay. *In vivo* virus growth kinetics results showed that ZIKV SW01 replicated to a peak level of 10^6 PFU/mL on day 8, and then gradually declined to around 10^4 PFU/mL on day 12 (Supplementary Fig. S1A). Therefore, the day 8 viral stock was used to infect new DP2 neonatal mice, from which viruses were harvested again from the brain on day 8 and used to infect another DP2 neonatal mice. After repeating this process for 11 rounds, we obtained a mouse adapted virus, and named herein as MA-SW01 (or MA-P11) (Supplementary Fig. S1B). To characterize the mouse adapted ZIKV, 100 PFU of parental SW01 virus, mouse adapted MA-SW01 virus, or negative control sterile PBS were i.c. injected into DP2 newborn BALB/c mice and monitored for up to 25 days. All mice in the SW01 group showed a slow and moderate disease progression within 11–25 days (Fig. 1B and C), in comparison, those in the MA-SW01 group showed severe morbidity, and even death within 6–8 days (Fig. 1B, D); indicating MA-SW01 is more virulent than SW01. To determine whether the above effects are viral specific, a dose-response infection experiment was performed. Different groups of DP2 BALB/c mice were i.c. inoculated with 0.1, 1, or 10 PFU of SW01 virus or mouse adapted MA-SW01 virus, or sterile PBS control, and then monitored for 25 days. Results showed that at 1 or 10 PFU of MA-SW01, 100% of mice died within 7–9 days; in contrast, 1 PFU of SW01 was not lethal, and 10 PFU of SW01 only caused 77.8% fatality within a much longer period of 22–23 days. Of note, even at 0.1 PFU, 62.5% mice in the MA-SW01 group died within 10–11 days post infection, and the remaining 37.5% survived for 25 days, the entire duration of observation; but the same dose of 0.1 PFU of SW01 did not cause any death (Supplementary Fig. S2A). These data demonstrated that MA-SW01 is more virulent than the parental strain and it impacts on viral pathogenesis in a dose dependent manner.

To mimic natural ZIKV infection, 100 PFU of the parental SW01 virus or mouse adapted MA-SW01 virus was injected subcutaneously (s.c.) to DP2 and DP7 BALB/c mice and monitored for survival changes over time. Results showed that infection by the parental SW01 virus was nonlethal to either DP2 or DP7 mice; in contrast, inoculation with the mouse adapted MA-SW01 virus caused 100% mortality in DP2 mice within 6–8 days, and 25% death in DP7 mice at 15 days post infection (Supplementary Fig. S2B). Together with previous results (Fig. 1B), these data indicate that the virulence of MA-SW01 is age-dependent, but unrelated
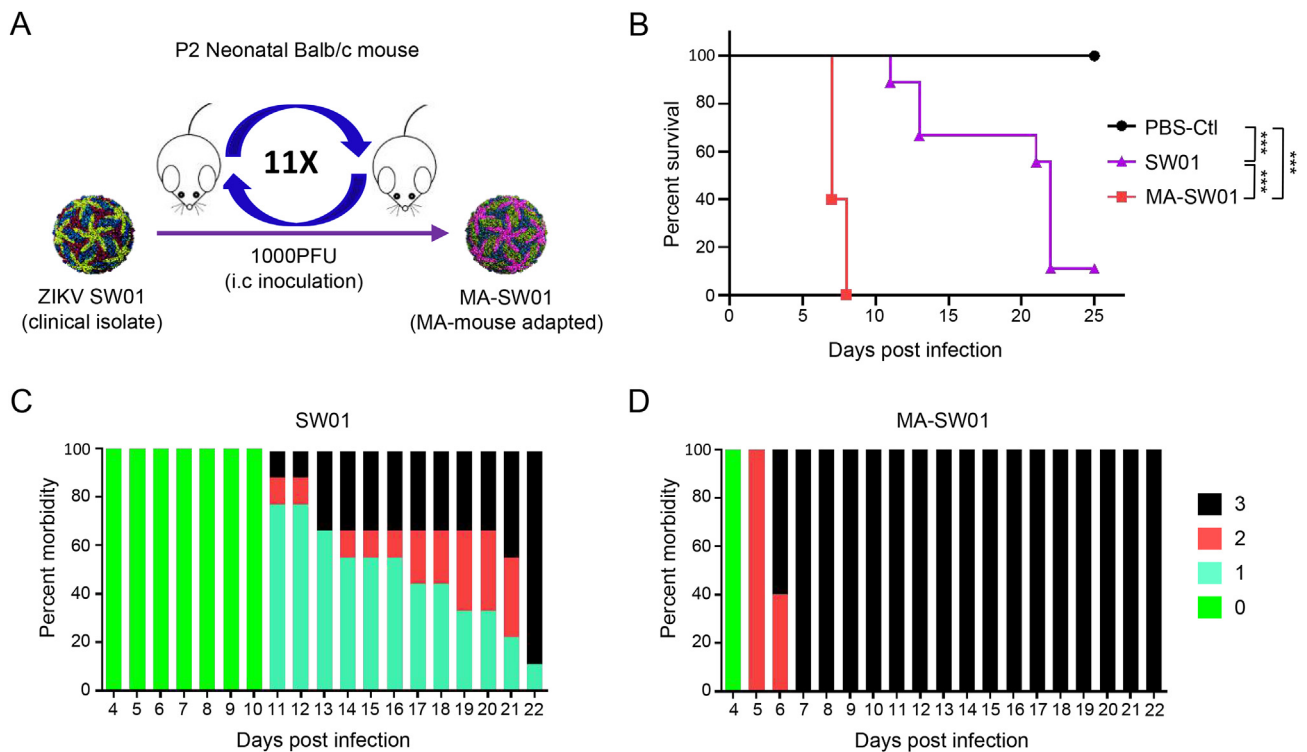
Fig. 1. *In vivo* adaptation of ZIKV clinical isolate SW01 increases virus virulence. **A** Schema of ZIKV *in vivo* passaging model; homogenate supernatant of infected mouse brain at 8 dpi was collected and used for the next round infection in naïve DP2 BALB/c mice. This process was repeated for 11 rounds to obtain a mouse adaptive virus MA-SW01. **B–D** DP2 BALB/c mice were injected i.c. with 100 PFU SW01, MA-SW01, or PBS (n=9–10 for each group). **B** Survival was monitored from 0 to 25 days post infection; **C–D** The morbidity of SW01 and MA-SW01 infected mice (clinical score: 0-healthy, 1-manic and limb weakness, 2-limb paralysis, 3-moribund or death); Survival rate were analyzed by log rank test; *P* values were indicated by *** (*P* < 0.001). Data shown are representative of two independent experiments.

to the route of infection. To examine whether the increased virulence of MA-SW01 virus is reproducible on other mouse strain, we next infected DP2 C57BL/6 mice with either SW01 or MA-SW01 virus, and then monitored them for 15 days. Results showed that MA-SW01 infected C57BL/6 mice exhibited 100% mortality between 6 and 7 days post infection, whereas only 44.4% of the SW01 infected mice died within 15 days of infection (Supplementary Fig. S3). Thus, the increased virulence of mouse adapted MA-SW01 virus is not restricted to one specific mouse genetic background.

3.2. MA-SW01 replicates significantly better in brain and other organs

A low-dose ZIKV infection ($2{\times}10^3$ PFU) in C57BL/6 neonates can cause a limited but detectable level of infection in mouse brain, but resulted lower mortality than that in immunodeficient A6 mice (Mana-ngeeswaran et al., 2016); a high-dose infection (10^6 TCID50) in C57BL/6 neonates, however, led to systemic infection and 100% death (Li et al., 2018). To examine whether the mouse adapted MA-SW01 virus can cause increased pathology, DP2 BALB/c mice were infected s.c. with parental SW01 virus or MA-SW01 virus, and then the viral loads in tissues including brain, eyes, blood, spleen, and kidney were quantified by real time-qPCR at 3- and 6-days post infection. Results showed that higher level of virus RNA was detected in the brain of MA-SW01 infected mice than that of SW-01 infected mice at 3 days post infection, and higher viral loads in multiple tissues (brain, eye, blood, and spleen) were observed in MA-SW01 infected mice than that in SW01 infected mice at 6 days post infection (Fig. 2A). Specifically, the average viral RNA level in the brain of MA-SW01 infected mice was about 15-fold and 488-fold higher than that of SW01 infected mice at 3- and 6-days post infection, respectively. At 6 days post infection, the viral RNA level in eyes of MA-SW01 infected mice was 22-fold higher than that of SW01 infected mice; the viral RNA

level in spleen of MA-SW01 infected mice was 5-fold higher than that of SW01 infected mice; the viral RNA level in blood of MA-SW01 infected mice was 54-fold higher than that of mice infected by SW01 virus (Fig. 2A).

The fact that the viral load in the brain of MA-SW01 infected mice was more than 400-fold (488-fold to be exact) higher than that of SW01 infected mice at day 6 post infection suggests two possibilities: one is that MA-SW01 virus replicates overall more efficiently than SW01 in the central nerve system (CNS); another is that more MA-SW01 virus has entered CNS than SW01 because of increased capacity of neuro-invasion. To differentiate between these two possibilities, DP2 BALB/c mice were infected with 100 PFU of SW01 virus or MA-SW01 virus by intracranial (i.c.) inoculation and viral RNA in the brains were quantified by real-time qPCR. Results showed that viral RNA of MA-SW01 group was initially not significantly different from that of SW01 group at 3 days post infection (Fig. 2B) but became 13.8-fold higher than that of SW01 group at 6 days post infection (Fig. 2C), suggesting more efficient replication of MA-SW01 in the brain. Given that viral RNA level in the brain of MA-SW01 group was about 15-fold higher than that of SW01 group at day 3, even with s.c. inoculation (Fig. 2A), we deduced that the more virulent MA-SW01 virus also has greater penetration to brain. To visualize viral infection more directly in the brain, immunofluorescence staining of virus E protein in brain tissue sections was performed. Dramatically stronger fluorescent intensity was detected in brains of MA-SW01 infected mice than that in SW01 infected mice at 6 days post infection (Fig. 2D). More detailed brain staining analyses showed that the cortex and hippocampus regions are major sites for MA-SW01 infection (Supplementary Fig. S4), albeit the specific target cells in these tissues are currently unclear. Collectively, the above data indicate that MA-SW01 virus has both greater replicative ability in CNS cells and increased tropism for neuronal tissues.
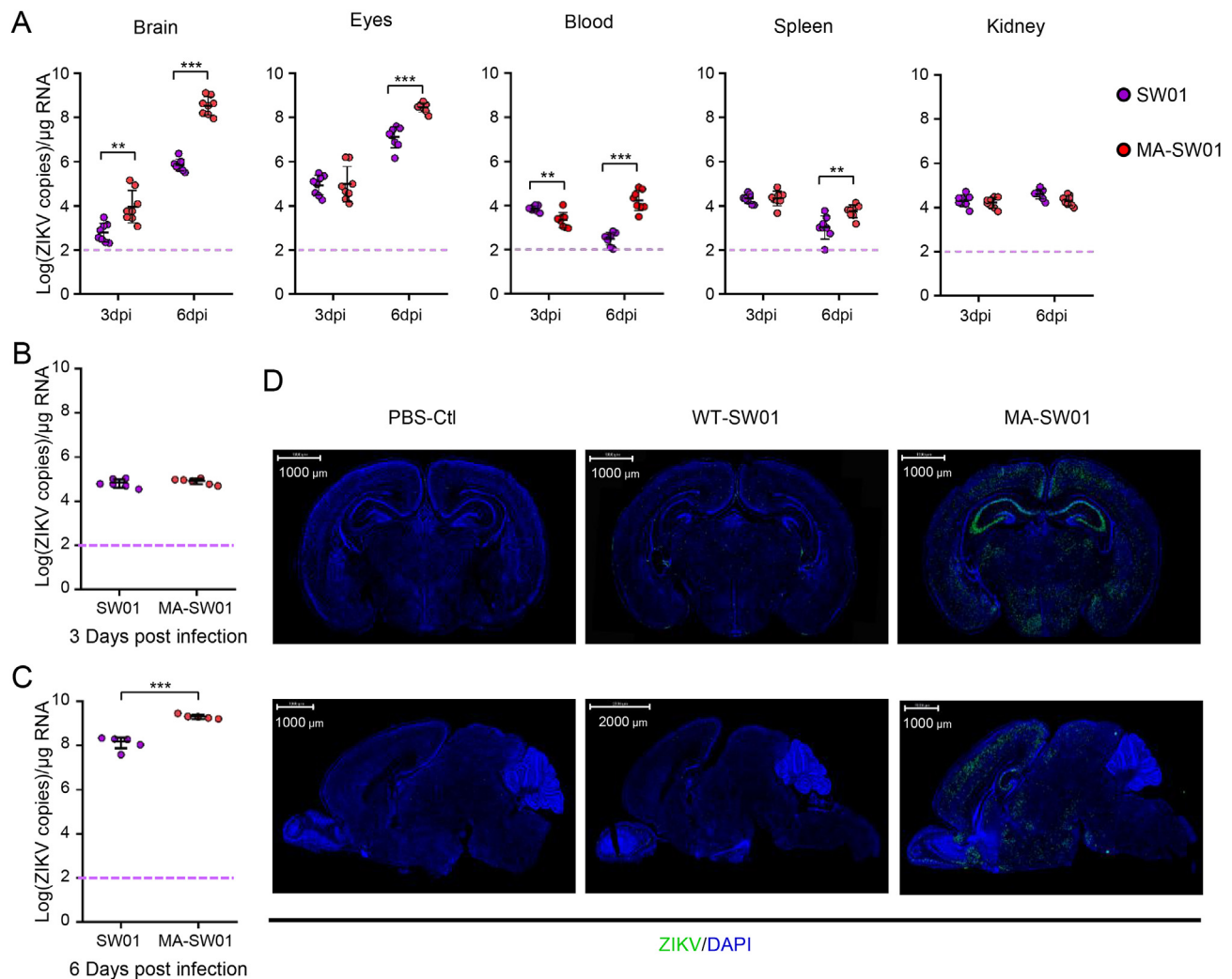
Fig. 2. Increased virulence of MA-SW01 is associated with elevated neurotropism. **A** DP2 BALB/c mice were infected s.c. with 100 PFU SW01 or MA-SW01 virus (n = 8 for each group). Virus RNA loads in tissues (brain, blood, spleen, liver and kidney) at 3 days post infection (3 dpi) and 6 days post infection (6 dpi) after infection were determinated by real-time PCR; dotted lines denote the limit of detection of the real-time PCR. **B–C** DP2 BALB/c mice were infected i.c. with 100 PFU SW01 or MA-SW01 virus (n = 5–6 for each group). Virus loads of brain at 3 dpi and 6 dpi was determined by real-time PCR; **D** DP2 BALB/c mice were infected s.c. with 100 PFU SW01 or MA-SW01 virus. Representative viral E protein expression in whole brain (both coronal and sagittal dissection) at 6 days post infection was detected by fluorescence immunoassay (IFA); The summary data were presented as mean ± standard deviation (SD) and analyzed by student's *t*-test; *P* values were indicated by ** (*P* < 0.01), or *** (*P* < 0.001). Data shown are representative of two independent experiments.

3.3. The MA-SW01 virus has four high frequency nonsynonymous mutations

To exploit whether the increased virulence of mouse adapted MA-SW01 virus is a reflection of unique genetic characteristics of a virus clone or the collective property of viral quasispecies, we compared the MA-SW01 virus with its parental virus SW01 at the phenotypic and genetic levels. Biological clones derived from MA-SW01 virus (MA-1 to MA-10) were found to be more virulent than clones from SW01 (SW-1 to SW-4) (Supplementary Fig. S5), indicating the increased virulence of MA-SW01 is not a reflection of viral quasispecies but may be related to single viral clones with specific genetic characteristics. To uncover the genetic features, total RNA was extracted from the original SW01 viral stock and mouse adapted MA-SW01 virus, and then subjected to the next generation sequencing. Intrahost single nucleotide variant (iSNV) across the whole genome was analyzed by CLC genomic workbench. Results showed a total of 6 nucleotide substitutions (G1069A, G1074A, C1089T, A1330G, G3787A and T6036C) over 80% reads in the open reading frame (ORF) of mouse adapted MA-SW01 virus (Fig. 3A). Among these substitutions, four were nonsynonymous mutations (G1069A, G1074A,

A1330G and G3787A), and two were synonymous mutations (C1089T and T6036C); the four nonsynonymous mutations led to three amino acid changes on virus E protein (D67N, M68I, N154D), and one on NS2A protein (A117T) (Fig. 3B). Of note, N154 is a unique glycosylation site on E protein, and it has been shown to support ZIKV infection in adult immunodeficient mice through either enhancing virus neuroinvasion or facilitating DC-SIGN binding (Annamalai Arun et al., 2017; Carbaugh Derek et al., 2019). However, when inoculated i.c. into neonatal mice, ZIKV with N154 glycosylation deletion had no decrease in virulence (Fontes-Garfias et al., 2017). Collectively, these published data suggest that the N154D mutation may not be linked to the augmented infectivity and increased neurovirulence we have observed for the mouse adapted MA-SW01 virus. Hence, we focused on the other three amino acid mutations (D67N, M68I on E protein, and A117T on NS2A protein) for further investigation.

3.4. Mutations on E protein are required for increased virus virulence

On the backbone of ZIKV infectious clone pFLZIKV (Shan et al., 2016), three mutant viruses (CM1, CM2 and CM3) were constructed:
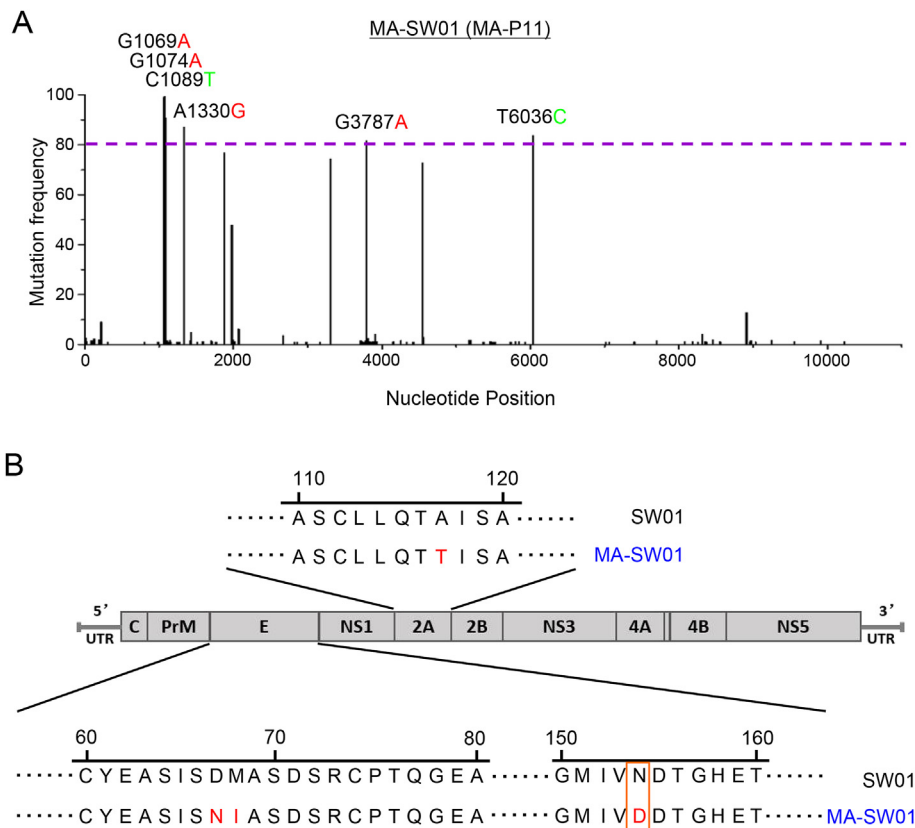
Fig. 3. NGS analyses of the MA-SW01 virus identify four high frequency nonsynonymous mutations on E and NS2A genes. **A–B** Virus RNA extracted from SW01 and MA-SW01 was used to construct the sequence library, and then sequenced by the next generation sequencing (NGS) method. Quantification and plotting of mutation frequency were performed by CLC Genomic Workbench and Origin software. **A** Plots of missense mutations frequency across the ORF of MA-SW01 in reference to consensus sequence of SW01; nucleotides with frequency higher than 80% reads were shown (red nucleotide abbreviations represent missense mutations, and green ones are silent mutations). Dotted lines denote the frequency of 80%. **B** Amino acid changes corresponding to missense mutations.

CM1 includes D67N and M68I mutations on E protein; CM2 includes the A117T mutation on NS2A protein; CM3 contains all three substitutions on E and NS2A proteins (Fig. 4A). In BHK-21 cells, 1–3 days after transfection with *in vitro* transcribed RNA from these viral constructs, ZIKV E protein expression was examined with a monoclonal antibody. Results showed that all three molecularly cloned mutant viruses were rescued and replicated efficiently (Fig. 4B). These molecularly cloned mutant viruses were then used to infect DP2 BALB/c mice i.c. at 10 PFU/mouse, with the parental CAM-WT virus as a control, and then monitored for 25 days. Results showed that CM1 and CM3, but not CM2, are more virulent than CAM-WT (Fig. 4C). Since both CM1 and CM3 contain 2 mutations on E protein (D67N, M68I), and CM2 only contains a single NS2A mutation, the above results suggest that the E protein mutations are determinants of increased virulence of MA-SW01, while the NS2A mutation is not. Therefore, CM1 virus which contains two E protein mutations was chosen for further investigation.

We next examined whether the route of infection alters viral virulence. DP2 BALB/c mice were infected s.c. with 100 PFU of control CAM-WT or test CM1 virus, and then monitored for up to 25 days. Results showed that CM1 infection led to higher mortality than that of CAM-WT (Fig. 4D). Although a difference was not observed at 3 days post infection (Fig. 4E), body weights of CM1 infected mice were significantly lighter than those infected by CAM-WT at 11 days post infection (Fig. 4F). Notably, disease progression appeared to be reversible in the control CAM-WT group, but not so in the CM1 group which had 100% mortality at 17 days post infection (Fig. 4G and H). These data demonstrated that both i.c. and s.c. inoculation of CM1 led to severe disease outcome.

Since virulence of the mouse adapted MA-SW01 virus was not restricted to a single mouse strain, we sought to confirm that the molecularly cloned CM1 virus follows the same principle. DP2 C57BL/6 mice were inoculated s.c. with 100 PFU of parental CAM-WT or test CM1, or negative control PBS, and then monitored for 25 days. All mice (100%) infected by CM1 virus died on 11–13 days post infection, whereas only 20% of those infected by CAM-WT succumbed after 25 days

(Supplementary Fig. S6). These data demonstrated that the virulent phenotype of CM1 is not limited to one mouse strain.

3.5. A D67N single amino acid mutation is sufficient to confer the increased virulence of CM1 virus

To determine which mutation of E protein is more critical for a major change in viral phenotype, we first analyzed single nucleotide variants in E protein sequence from serially passaged viruses from P1 (MA-P1) to P11 (MA-P11). Results revealed that there were progressive accumulations of D67N (from 22.7% to 99.4%), and M68I (from 3.0% to 91.7%) mutations during the *in vivo* serial passage of the parental SW01 virus. The baseline frequencies of these two mutations in the parental virus (P0, or SW01) were lower than 1%. Of note, the D67N maintained high mutation frequency (>90%) from P5 to P11 during *in vivo* passage (Fig. 5A). Consistent with the notion that this mutation may be functionally significant, DP2 C57BL/6 mice infected with 100 PFU of MA-P5, MA-P8 or MA-P10 showed 100% mortality at 10 days post infection, whereas the parental SW01 virus infected mice had only 16.7% mortality at 15 days post infection (Fig. 5B). Given that the D67N mutation rapidly increased to 92.4% in P5 virus (Fig. 5A), and all single biological clones of the mouse adapted MA-SW01 virus contain the D67N mutation (Supplementary Table S1), it is reasonable to deduce that D67N mutation alone is responsible for the increased viral virulence. To test this idea, a molecular clone contains the single D67N mutation was constructed based on the CAM-WT backbone (pFLZIKV), and herein named CM1-A virus (Fig. 5C), which was rescued successfully as shown by immunofluorescence staining of ZIKV E protein in BHK-21 cells transfected with *in vitro* transcribed RNA (Fig. 5D). Then, 100 PFU of CM1, CM1-A virus, or PBS was inoculated s.c. into DP2 C57BL/6 mice that were monitored for up to 25 days. Results showed that CM1-A was similar to CM1 in causing 100% mortality of infected mice at 12–13 days post infection (Fig. 5E). These data demonstrated that a single D67N mutation is sufficient to account for the increased virulence of CM1.
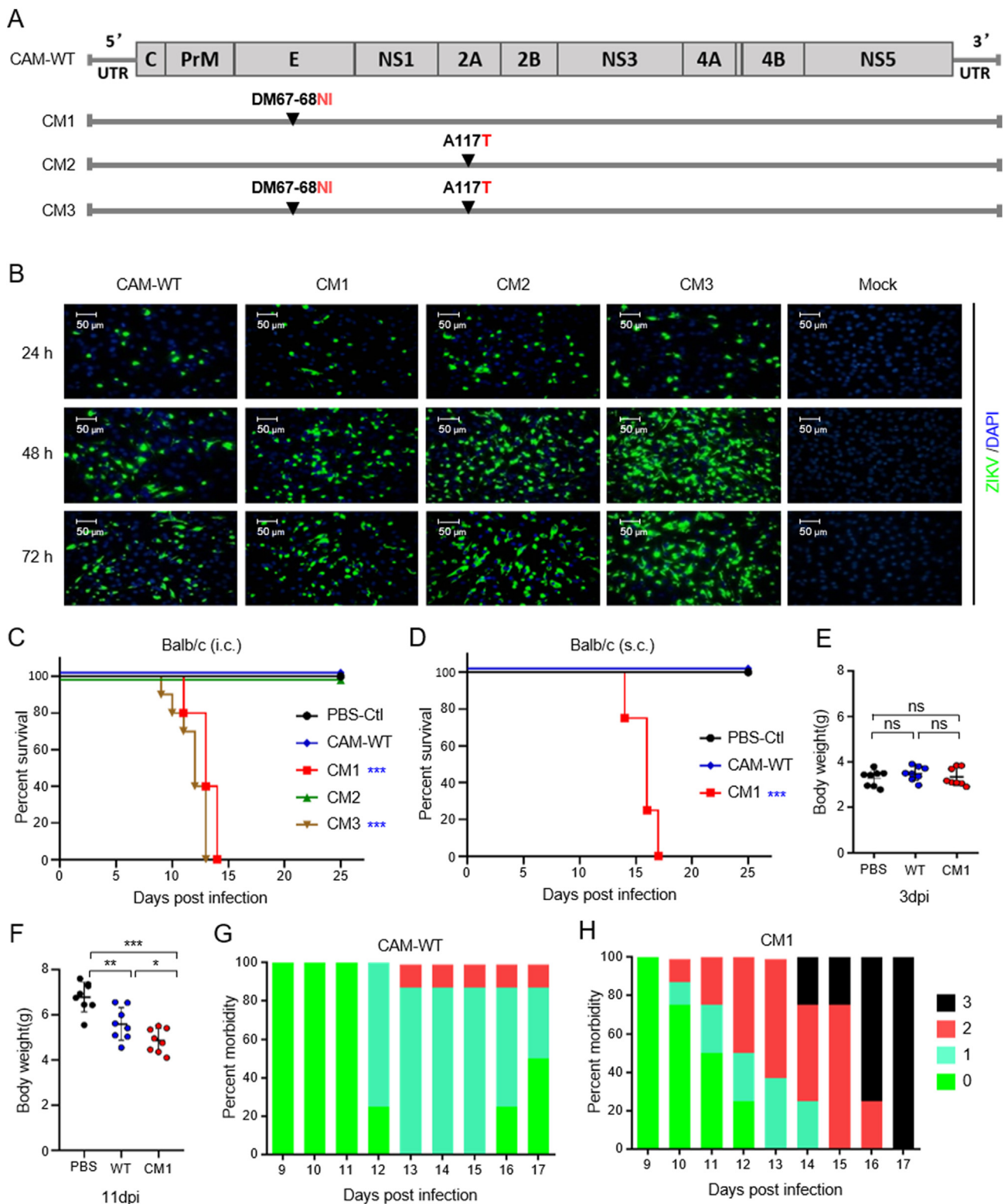
Fig. 4. Increased virulence of ZIKV in association with specific mutations on E protein but not on NS2A protein. **A** Scheme of mutation strategy based on pFLZIKV (CAM-WT) infectious clone to create CAM-M1 (CM1), CAM-M2 (CM2), CAM-M3 (CM3) viruses; **B** IFA of ZIKV E protein expression at indicated times (24, 48, 72 h post transfection) in BHK-21 cells transfected with RNA from CAM- WT or mutant viruses (CM1, CM2, CM3). **C** Survival curve of DP2 BALB/c mice infected i.c. with 10 PFU CAM-WT, mutant viruses (CM1, CM2, CM3), or PBS (n = 10 for each group). **D–H**. DP2 BALB/c mice were infected s.c. with 100 PFU CAM-WT, mutant viruses, or PBS (n = 8 for each group). **D** Survival was monitored and analyzed from 0 to 25 days post infection; **E–F**. Body weight difference between PBS-Ctl (PBS), CAM-WT (WT) and CAM-M1 (CM1) groups at 3- and 11-days post infection (3 dpi and 11 dpi); **G–H** The morbidity of CAM-WT and CAM-M1 groups (clinical score: 0-healthy, 1-manic and limb weakness, 2-limb paralysis, 3-moribund or death); the summary data were presented as mean ± standard deviation (SD) and analyzed by student's *t*-test; Survival rate was analyzed by log rank test; *P* values were indicated by * (*P* < 0.05), or ** (*P* < 0.01), or *** (*P* < 0.001). Data shown are representative of two independent experiments.
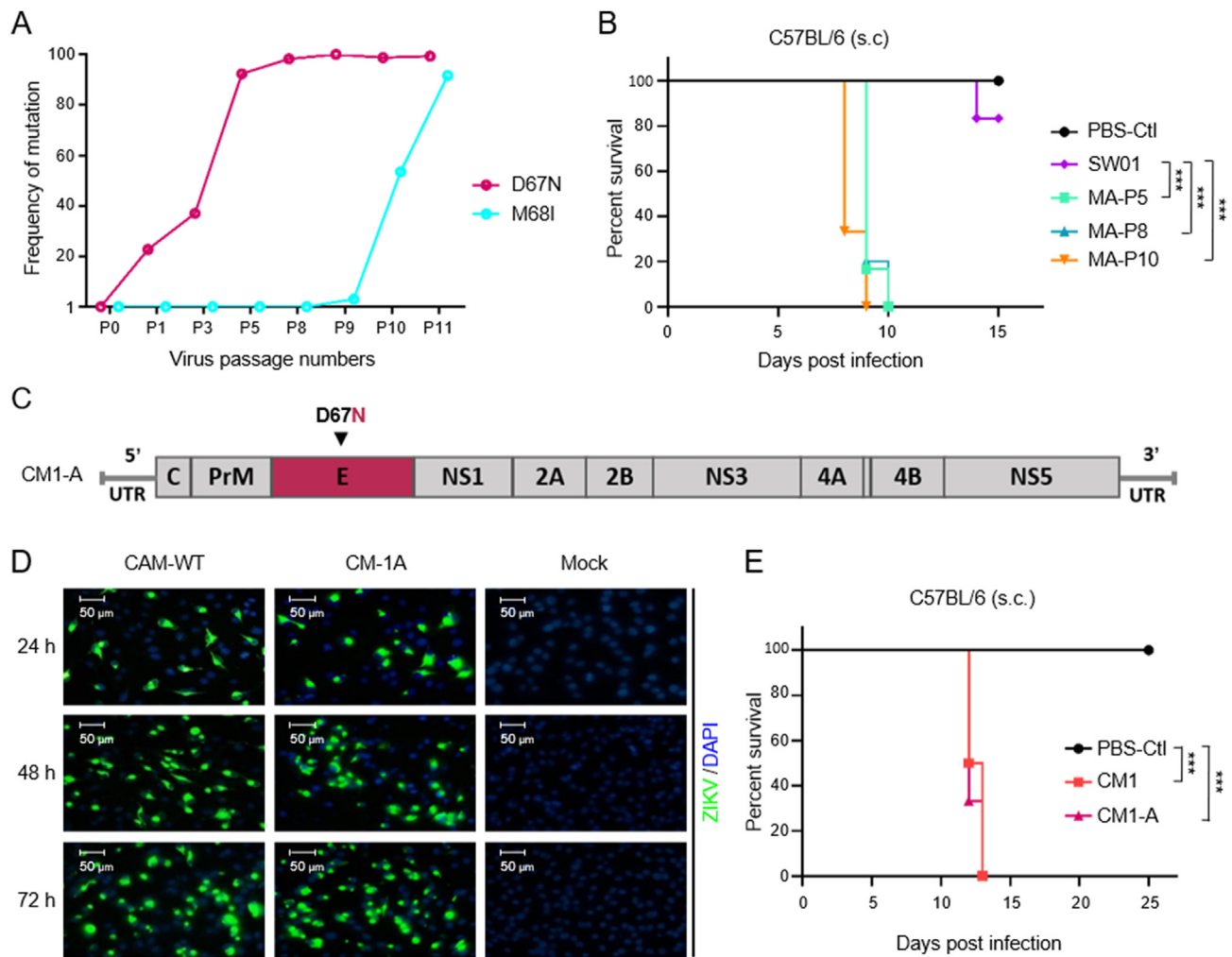
Fig. 5. Increased virulence of ZIKV is associated with a D67N single mutation on E protein. **A** Progressive changes of mutation frequency of 67 and 68 amino acids in E protein from SW01 (P0) to MA-SW01 (MA-P11) during *in vivo* passaging. **B** Survival curve of DP2 C57BL/6 mice infected s.c. with 100 PFU SW01, MA-P5, MA-P8, MA-P10, or PBS (n = 6–10 for each group). **C** Strategy to construct a single D67N substitution virus (CM1-A) based on pFLZIKV; (**D**) IFA of ZIKV E protein expression at indicated times (24, 48, 72 h post transfection) in BHK-21 cells transfected with RNA from CAM-WT and CM1-A. **E** Survival curve of DP2 C57BL/6 mice inoculated s.c. with 100 PFU CM1, CM1A virus, or PBS (n = 8–9 for each group). Survival rate was analyzed by log rank test; *P* values were indicated by *** (*P* < 0.001). Data shown are representative of two independent experiments.

3.6. D67N mutation on E protein promotes ZIKV infection in brain tissue

To investigate whether viral E protein mutations (D67N, M68I) in-fluence tissue tropisms, DP2 BALB/c mice were infected s.c. with either parental CAM-WT or test CM1 (containing both D67N, M68I), then euthanatized at 3- or 11-days post infection. Viral RNA in tissues were quantified by qRT-PCR. At 3 days post infection, all tissues except for eyes showed similar levels of viral RNA in both CAM-WT and CM1 groups; at 11 days post infection, however, viral RNA of CM1 group was significantly higher than that of CAM-WT group in brains, eyes and blood, but not in spleens and kidneys (Fig. 6A), confirming these E protein mutations affect tissue tropism.

The fact that more viral RNA was detected in brain and eyes, that are rich in nerve cells susceptible to ZIKV infection, implies that CM1 virus has growth advantage over CAM-WT in these cells. To directly test this notion, DP2 BALB/c mice were infected i.c. with CAM-WT or CM1, and then monitored for virus burden. Results showed that brain viral loads of CM1 group was higher than that of CAM-WT group at 11 days post infection, but not at 3 days post infection (Fig. 6B and C), confirming that CM1 has growth advantage over CAM-WT in brain.

To further dissect whether the single D67N mutation in E protein plays an essential role of altering viral virulence and tissue tropism, we

next used CM1-A virus (containing only D67N) to perform viral infection experiments in neonatal mice. Results showed that irrespective of i.c. infection (Fig. 6B and C), or s.c. infection (Fig. 6D), viral loads in brains of CM1-A infected mice were always higher than that of CAM-WT group at 11 days post infection, but not at 3 days post infection. Collectively, these data prove that the D67N mutation is sufficient to increase virus repli-cation in CNS.

3.7. Mutant virus infection causes more damage to human neural cells

Recent studies of SARS-CoV-2 virus have shown the emergence of convergent mutations in animal model and in human transmission conferring increasing infectivity or pathogenity (Luan et al., 2021; Zhou et al., 2021). To further test if this D67N mutation increases ZIKV infectivity, different types of cells were infected with wild type ZIKV CAM-WT or D67N mutant ZIKV CM1-A. Results showed that CM1-A infection causes more severe cytopathic effect (CPE) than CAM-WT to human neural astrocytes (U251), but not to monkey kidney epithelial cells (Vero), human lung epithelial cells (A549), and mosquito cells (C6/36) (Fig. 7A). Besides, virus titers in supernatants from CM1-A infected U251 cells are higher than that from CAM-WT infected cells (Fig. 7B). Since astrocytes exist congruously in the cortex and
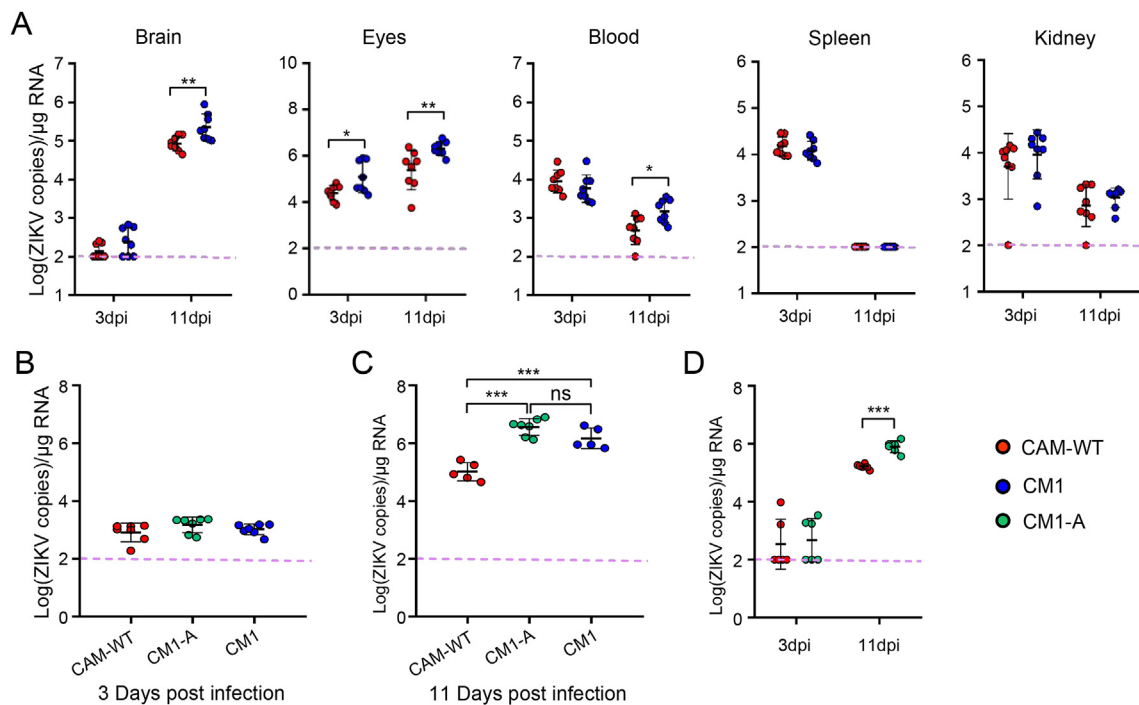
Fig. 6. Molecularly cloned ZIKV with a D67N single mutation on E protein has marked increase in the infection of brain tissues. **A** DP2 BALB/c mice were infected s.c. with 100 PFU CAM-WT or CM1 (n = 8 for each group). Virus RNA loads in tissues (brain, blood, spleen, liver and kidney) at 3 days post infection (3 dpi) and 11 days post infection (11 dpi) were determined by real-time PCR; **B–C** DP2 BALB/c mice were infected i.c. with 20 PFU CAM-WT, CM1 and CM1-A (n = 5–7 for each group). Virus RNA load in brains at 3 dpi (**B**) and 11 dpi (**C**) were determined by real-time PCR; **D** DP2 BALB/c mice were infected s.c. with 100 PFU CAM-WT or CM1-A (n = 6 for each group). Virus RNA loads in brains at 3 dpi and 11 dpi were determined by real time PCR; The summary data were presented as mean ± standard deviation (SD) and analyzed by student's *t*-test; *P* values were indicated by * (*P* < 0.05), or ** (*P* < 0.01), or *** (*P* < 0.001). Data shown are representative of two independent experiments.
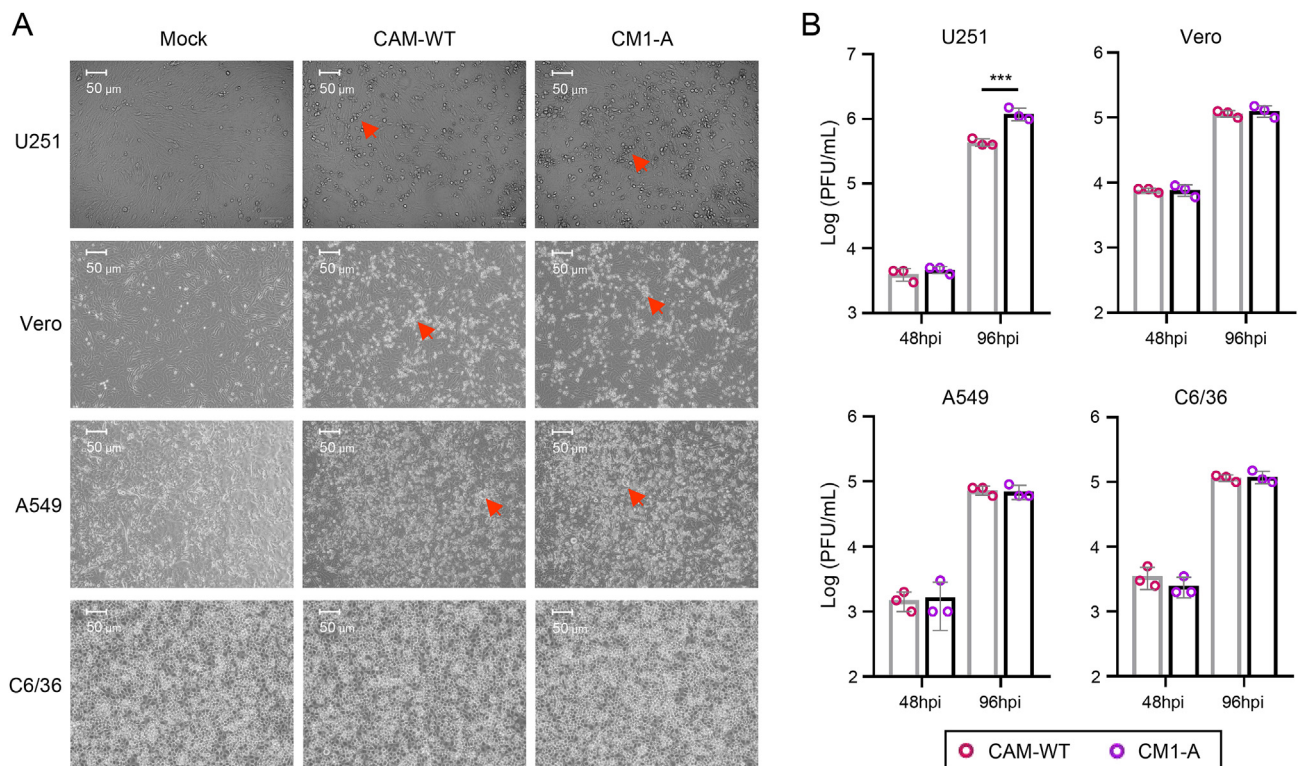

Fig. 7. Mutant virus infection causes more damage to human neural U251 cells. U251, Vero, A549 and C6/36 cells were infected with CAM-WT virus or CM1-A virus, at MOI of 0.1 (n = 3 for each group); **A** Cell morphology and cytopathic effect (CPE) was recorded by camera at 48 h post infection (for Vero, A549 and C6/36 cells) or 96 h post infection (for U251 cells). The red arrow points to the CPE. No obvious CPE was observed for infected C6/36 cells. **B** Virus titer of supernatants from CAM-WT or CM1-A infected cells (MOI of 0.1) at 48 or 96 h post infection (hpi) was titrated by plaque assay. Data shown are representative of two independent experiments.

Table 1
Deduced amino acid polymorphism at the 67 site of ZIKV E protein of WT-SW01 strain.

Reads[a] (1069 of ORF)	Nucleotide polymorphism (1069 of ORF)	Amino acid polymorphism (67 of Envelope)	Percentage of total Reads
18167	1069(G,T,C)	67(Asp, Tyr, His)	99.945%
10	1069(A)	67(Asn)[b]	0.055%

[a] Based on deep sequencing;
[b] The D67N mutation presents at low frequency in the original viral isolate.

hippocampus regions of humans and mice (Batiuk et al., 2020; Vasile et al., 2017), it is reasonable to deduce that astrocytes are the potential target cells of D67N mutant ZIKV. Collectively, these data suggest that ZIKV variant containing D67N mutation may cause severe neurological infection to humans when emerging naturally.

3.8. Rapid D67N accumulation may have increased virus fitness

To examine whether the D67N substitution in mouse adapted MA-SW01 virus was originated from the parental clinical isolate SW01 virus, or resulted from an extraneous selection process, we analyzed the polymorphism of nucleotide at the 1069 position of SW01 open reading frame (ORF) which corresponds to amino acid sequence at the 67 position of E protein. Results show that the 1069A variant of ORF (D67N) was present in the initial SW01 stock at a low frequency of 0.055% and rapidly raised to 22.7% after being passaged once in mouse brain (Table 1), then progressively increased to more than 90% at passage 5 (Fig. 5A). This indicates that viral quasispecies features the N67 on its E protein constituted a minority of viruses. Besides, CM1-A has growth advantage in neuro U251 cells over CAM-WT (Fig. 7B). Collectively, it is reasonably to deduce that D67N substitution on mouse adapted MA-SW01 provides more viral fitness in CNS, it enables MA-SW01 to outgrow other viral variants within the original SW01 quasispecies during serial passaging.

4. Discussion

Viral sequence variations can result in profound changes on its interaction with human cells, and possibly altering disease progression. This has been demonstrated some years ago with HIV in which small amino acids change on the Env protein led to great viral tropism change from T-cell tropic to macrophage tropic (Cheng-Mayer et al., 1988; Shioda et al., 1991; Shioda et al., 1992). Differences in viral tropism have clear impact on HIV disease progression (Fauci, 1996; Levy, 2009), as having been convincingly demonstrated *in vivo* using a nonhuman primate model of SHIV infection (Harouse et al., 1999). More recently, amino acid changes on SARS-CoV-2 have been used to sort viruses into clusters that originated COVID-19 outbreaks in different countries (Forster et al., 2020). In order to understand why ZIKV infection caused neurological diseases only in some infected individuals, we tested the hypothesis that unique genetic variant of the virus is associated with increased neurovirulence.

By serial passage of a clinical isolate of ZIKV SW01 in the brains of neonatal mice, we have generated a mouse adapted MA-SW01 strain that showed 100–1000-fold increased virulence than its parental virus, with corresponding increase in neurotropism. NGS analyses revealed that the MA-SW01 virus has four dominant nonsynonymous nucleotide mutations on genes encoding E protein (three mutations) and NS2A protein (one mutation). Using molecularly cloned viral variants containing these mutations either singly or in combination, we demonstrated that a single G to A nucleotide mutation at position 1069 of ZIKV ORF that correspond to an Aspartic acid (Asp, D) to an Asparagine (Asn, N) amino acid change on position 67 of the E protein (D67N) is sufficient to confer greater viral replication in mouse brain and significantly increased mortality. These

results not only establish an *in vivo* model by which many facets of ZIKV pathogenesis could be further studied, but also provide a tangible viral genetic basis to explain the neurological complications observed in recent large ZIKV outbreaks.

Identifying viral genetical features that may affect the outcomes of viral infections or reveal the origin of virus is an area of significant scientific interest (Cheng-Mayer et al., 1988; Fauci, 1996; Forster et al., 2020; Harouse et al., 1999; Levy, 2009; Shioda et al., 1991; Shioda et al., 1992). ZIKV with mutations on prM, NS1, NS4B have been reported to profoundly change viral infectivity in mosquitoes, cell lines, and mice (Gorman et al., 2018; Liu et al., 2017; Yuan et al., 2017). In the current study, we discovered a new mutation on E protein that markedly increased ZIKV's neurovirulence.

Our findings have immediate implications. The D67 on E protein is conserved among many ZIKV strains, and it may be functionally important. Similarly, in all four DENV serotypes, there are two highly conserved *N*-linked glycosylation sites on E protein, N67 and N153, that play critical role for viral entry (Rey, 2003). Indeed, several monoclonal antibodies (mAbs) targeting this site have been isolated from ZIKV-infected patients, and shown to be capable of preventing ZIKV infection in animal models (Long et al., 2019; Niu et al., 2019; Sapparapu et al., 2016; Wang et al., 2016). It would be interesting to test in future studies whether D67N mutant virus can escape these antibodies, and thereby become more virulent. With respect to the N154 glycosylation site on E protein, our data raise some concerns about the strategy of preparing an attenuated ZIKV vaccine by introducing deletion of N154 glycosylation; such an attenuated virus has decreased infectivity and neuroinvasion in mice, while maintaining immunogenicity of viral antigens (Fontes-Garfias et al., 2017). We found that mouse adapted MA-SW01 virus being highly virulent despite lacking a N154 glycosylation sequence motif, even more than viruses cloned from the parental SW01 virus and those contain intact N154 glycosylation site. Therefore, the vaccine strategy utilizing a deletion of N154 glycosylation may only apply to some viral variants but not others, and such a strategy must be used judiciously.

Why a single D67N mutation on E protein can dramatically change ZIKV tropism and infectivity is currently unknown. Its potential link to glycosylation needs to be considered first because the two highly conserved *N*-linked glycosylation sites, N67 and N153, are important for viral entry as demonstrated in all four DENV serotypes (Rey, 2003), and glycosylation on N153 or N154 of E protein helps West Nile virus (WNV) or Japanese encephalitis virus (JEV) to invade CNS in mammals (Beasley David et al., 2005; Liang et al., 2018). Similar to JEV, ZIKV has only one N154 glycosylation site on E protein without the N67 site (Fontes-Garfias et al., 2017; Hasan et al., 2018). However, an additional use of N67 glycosylation on JEV attenuates virus pathogenesis and reduces viral neuro-invasion *in vivo* (Liang et al., 2018), despite the N67 glycosylation mediates enhanced infectivity of WNV or DENV by facilitating interaction with DC-SIGN molecule on cell surface in cell culture models (Davis et al., 2006; Liang et al., 2018; Pokidysheva et al., 2006). An un-glycosylated N67 has been found on a number of flaviviruses (Barker et al., 2009), but its influence on pathogenesis is unknown. Because the mouse adapted MA-SW01 virus has a mutation on the N154 site and unable to acquire glycosylation through this site, it is tempting to suggest that the D67N is a functional compensatory mutation, an idea that could be tested in future studies. Another possible mechanism is that the D67N mutation had evolved to counteract with host antiviral immune responses.

5. Conclusions

In conclusion, we have identified a single amino acid mutation, D67N, on the putative glycosylation site of E protein of ZIKV and demonstrated that molecularly cloned virus with this mutation has markedly increased neurovirulence in mice and growth advantage in human neural cell line U251. Though this mutation has not been reported

in field ZIKV isolate yet, close monitoring and large-scale screening of this unique viral variant in humans should provide clue to understand some major questions in the field, such as the sudden outbreak of ZIKV disease in certain locale, and the association between ZIKV infection and neurological disorders.

Data availability

The authors declare that the data supporting the findings of this study are available within the article or upon request to the corresponding authors. The NGS raw data have been deposited in Sequence Read Archive (SRA) of NCBI (Access number: SRP237251).

Ethics statement

All experiments were performed strictly in accordance with the guidelines of care and use of laboratory animals by the Ministry of Science and Technology of the People's Republic of China and regulations of biosafety level 2 (BSL-2) and animal biosafety level-2 (A-BSL-2) containment facilities at Institut Pasteur of Shanghai. The experiment protocols to generate mouse adapted ZIKV were approved by Institut Pasteur of Shanghai (Approval number: A2018027). All mice used in this study were carefully fed and suffering of animals was minimized.

Author contributions

Zhihua Liu: conceptualization, data curation, formal analysis, investigation, methodology, software, visualization, writing – original draft, writing – review & editing. Yawei Zhang: data curation, formal analysis, investigation, methodology, software, validation. Mengli Cheng: data curation, investigation, methodology, validation. Ningning Ge: investigation, methodology. Jiayi Shu: methodology. Zhiheng Xu: methodology. Xiao Su: conceptualization, supervision. Zhihua Kou: conceptualization, project administration, supervision, visualization, writing – review & editing. Yigang Tong: conceptualization, resources. Chengfeng Qin: conceptualization, funding acquisition, resources. Xia Jin: conceptualization, funding acquisition, project administration, supervision, visualization, writing – review & editing.

Conflict of interest

The authors declare no conflicts of interest.

Acknowledgement

Appendix A. Supplementary data

Supplementary data to this article can be found online at https://doi.org/10.1016/j.virs.2022.01.021.

References

Annamalai Arun, S., Pattnaik, A., Sahoo Bikash, R., Muthukrishnan, E., Natarajan Sathish, K., Steffen, D., Vu Hiep, L.X., Delhon, G., Osorio Fernando, A., Petro Thomas, M., Xiang, S.-H., Pattnaik Asit, K., Diamond, Michael S., 2017. Zika virus encoding nonglycosylated envelope protein is attenuated and defective in neuroinvasion. J. Virol. 91 e01348-01317.

Auvin, S., Pressler, R., 2013. Comparison of brain maturation among species: an example in translational Research suggesting the possible use of bumetanide in newborn. Front. Neurol. 4.

Bardina, S.V., Bunduc, P., Tripathi, S., Duehr, J., Frere, J.J., Brown, J.A., Nachbagauer, R., Foster, G.A., Krysztof, D., Tortorella, D., Stramer, S.L., García-Sastre, A., Krammer, F., Lim, J.K., 2017. Enhancement of Zika virus pathogenesis by preexisting antiflavivirus immunity. Science 356, 175.

Barker, W.C., Mazumder, R., Vasudevan, S., Sagripanti, J.-L., Wu, C.H., 2009. Sequence signatures in envelope protein may determine whether flaviviruses produce hemorrhagic or encephalitic syndromes. Virus Gene. 39, 1–9.

Batiuk, M.Y., Martirosyan, A., Wahis, J., de Vin, F., Marneffe, C., Kusserow, C., Koeppen, J., Viana, J.F., Oliveira, J.F., Voet, T., Ponting, C.P., Belgard, T.G., Holt, M.G., 2020. Identification of region-specific astrocyte subtypes at single cell resolution. Nat. Commun. 11, 1220.

Baud, D., Gubler, D.J., Schaub, B., Lanteri, M.C., Musso, D., 2017. An update on Zika virus infection. Lancet 390, 2099–2109.

Beasley David, W.C., Whiteman Melissa, C., Zhang, S., Huang Claire, Y.H., Schneider Bradley, S., Smith Darci, R., Gromowski Gregory, D., Higgs, S., Kinney Richard, M., Barrett Alan, D.T., 2005. Envelope protein glycosylation status influences mouse neuroinvasion phenotype of genetic lineage 1 West Nile virus strains. J. Virol. 79, 8339–8347.

Bhatnagar, J., Rabeneck, D., Martines, R., Reagan-Steiner, S., Ermias, Y., Estetter, L.B.C., Suzuki, T., Ritter, J., Keating, M.K., Hale, G., Gary, J., Muehlenbachs, A., Lambert, A., Lanciotti, R., Oduyebo, T., Meaney-Delman, D., Bolaños, F., Saad, E.A.P., Shieh, W.-J., Zaki, S., 2017. Zika virus RNA replication and persistence in brain and placental tissue. Emerg. Infectious Disease J. 23, 405.

Brito, C.A.A., Henriques-Souza, A., Soares, C.R.P., Castanha, P.M.S., Machado, L.C., Pereira, M.R., Sobral, M.C.M., Lucena-Araujo, A.R., Wallau, G.L., Franca, R.F.O., 2018. Persistent detection of Zika virus RNA from an infant with severe microcephaly – a case report. BMC Infect. Dis. 18, 388.

Brown, J.A., Singh, G., Acklin, J.A., Lee, S., Duehr, J.E., Chokola, A.N., Frere, J.J., Hoffman, K.W., Foster, G.A., Krysztof, D., Cadagan, R., Jacobs, A.R., Stramer, S.L., Krammer, F., García-Sastre, A., Lim, J.K., 2019. Dengue virus immunity increases Zika virus-induced damage during pregnancy. Immunity 50, 751–762 e755.

Cao-Lormeau, V.-M., Roche, C., Teissier, A., Robin, E., Berry, A.-L., Mallet, H.-P., Sall, A.A., Musso, D., 2014. Zika virus, French Polynesia, South Pacific, 2013. Emerg. Infectious Disease J. 20, 1084.

Carbaugh Derek, L., Baric Ralph, S., Lazear Helen, M., Dermody, Terence S., 2019. Envelope protein glycosylation mediates Zika virus pathogenesis. J. Virol. 93, e00113–119.

Cheng-Mayer, C., Seto, D., Tateno, M., Levy, J.A., 1988. Biologic features of HIV-1 that correlate with virulence in the host. Science 240, 80.

Davis, C.W., Mattei, L.M., Nguyen, H.-Y., Ansarah-Sobrinho, C., Doms, R.W., Pierson, T.C., 2006. The location of asparagine-linked Glycans on West Nile Virions controls their interactions with CD209 (Dendritic cell-specific ICAM-3 grabbing nonintegrin). J. Biol. Chem. 281, 37183–37194.

Deng, C., Liu, S., Zhang, Q., Xu, M., Zhang, H., Gu, D., Shi, L., He, Ja, Xiao, G., Zhang, B., 2016. Isolation and characterization of Zika virus imported to China using C6/36 mosquito cells. Virol. Sin. 31, 176–179.

Dowall, S.D., Graham, V.A., Rayner, E., Atkinson, B., Hall, G., Watson, R.J., Bosworth, A., Bonney, L.C., Kitchen, S., Hewson, R., 2016. A susceptible mouse model for Zika virus infection. PLoS Neglected Trop. Dis. 10, e0004658.

Driggers, R.W., Ho, C.-Y., Korhonen, E.M., Kuivanen, S., Jääskeläinen, A.J., Smura, T., Rosenberg, A., Hill, D.A., DeBiasi, R.L., Vezina, G., Timofeev, J., Rodriguez, F.J., Levanov, L., Razak, J., Iyengar, P., Hennenfent, A., Kennedy, R., Lanciotti, R., du Plessis, A., Vapalahti, O., 2016. Zika virus infection with prolonged maternal viremia and fetal brain abnormalities. N. Engl. J. Med. 374, 2142–2151.

Duffy, M.R., Chen, T.-H., Hancock, W.T., Powers, A.M., Kool, J.L., Lanciotti, R.S., Pretrick, M., Marfel, M., Holzbauer, S., Dubray, C., Guillaumot, L., Griggs, A., Bel, M., Lambert, A.J., Laven, J., Kosoy, O., Panella, A., Biggerstaff, B.J., Fischer, M., Hayes, E.B., 2009. Zika virus outbreak on Yap Island, Federated States OF Micronesia. N. Engl. J. Med. 360, 2536–2543.

Fauci, A.S., 1996. Host factors and the pathogenesis of HIV-induced disease. Nature 384, 529–534.

Fontes-Garfias, C.R., Shan, C., Luo, H., Muruato, A.E., Medeiros, D.B.A., Mays, E., Xie, X., Zou, J., Roundy, C.M., Wakamiya, M., Rossi, S.L., Wang, T., Weaver, S.C., Shi, P.-Y., 2017. Functional analysis of glycosylation of Zika virus envelope protein. Cell Rep. 21, 1180–1190.

Forster, P., Forster, L., Renfrew, C., Forster, M., 2020. Phylogenetic network analysis of SARS-CoV-2 genomes. Proc. Natl. Acad. Sci. Unit. States Am. 117, 9241.

Gorman, M.J., Caine, E.A., Zaitsev, K., Begley, M.C., Weger-Lucarelli, J., Uccellini, M.B., Tripathi, S., Morrison, J., Yount, B.L., Dinnon III, K.H., Rückert, C., Young, M.C., Zhu, Z., Robertson, S.J., McNally, K.L., Ye, J., Cao, B., Mysorekar, I.U., Ebel, G.D., Baric, R.S., Best, S.M., Artyomov, M.N., Garcia-Sastre, A., Diamond, M.S., 2018. An immunocompetent mouse model of Zika virus infection. Cell Host Microbe 23, 672–685 e676.

Hanners Natasha, W., Eitson Jennifer, L., Usui, N., Richardson, R.B., Wexler Eric, M., Konopka, G., Schoggins John, W., 2016. Western Zika virus in human fetal neural progenitors persists long term with partial cytopathic and limited immunogenic effects. Cell Rep. 15, 2315–2322.

Harouse, J.M., Gettie, A., Tan, R.C.H., Blanchard, J., Cheng-Mayer, C., 1999. Distinct pathogenic Sequela in Rhesus Macaques infected with CCR5 or CXCR4 utilizing SHIVs. Science 284, 816.

Hasan, S.S., Sevvana, M., Kuhn, R.J., Rossmann, M.G., 2018. Structural biology of Zika virus and other flaviviruses. Nat. Struct. Mol. Biol. 25, 13–20.

Jouannic, J.-M., Friszer, S., Leparc-Goffart, I., Garel, C., Eyrolle-Guignot, D., 2016. Zika virus infection in French Polynesia. Lancet 387, 1051–1052.

Lazear Helen, M., Govero, J., Smith Amber, M., Platt Derek, J., Fernandez, E., Miner Jonathan, J., Diamond Michael, S., 2016. A mouse model of Zika virus pathogenesis. Cell Host Microbe 19, 720–730.

Levy, J.A., 2009. HIV pathogenesis: 25 years of progress and persistent challenges. AIDS 23.

Li, C., Xu, D., Ye, Q., Hong, S., Jiang, Y., Liu, X., Zhang, N., Shi, L., Qin, C.-F., Xu, Z., 2016. Zika virus disrupts neural progenitor development and leads to microcephaly in mice. Cell Stem Cell 19, 120–126.

Li, S., Armstrong, N., Zhao, H., Hou, W., Liu, J., Chen, C., Wan, J., Wang, W., Zhong, C., Liu, C., Zhu, H., Xia, N., Cheng, T., Tang, Q., 2018. Zika virus fatally infects wild type neonatal mice and replicates in central nervous system. Viruses 10, 49.

Liang, J.-J., Chou, M.-W., Lin, Y.-L., 2018. DC-SIGN binding contributed by an extra N-linked glycosylation on Japanese encephalitis virus envelope protein reduces the ability of viral brain invasion. Frontiers in Cellular and Infection Microbiology 8, 239.

Liu, Y., Liu, J., Du, S., Shan, C., Nie, K., Zhang, R., Li, X.-F., Zhang, R., Wang, T., Qin, C.-F., Wang, P., Shi, P.-Y., Cheng, G., 2017. Evolutionary enhancement of Zika virus infectivity in Aedes aegypti mosquitoes. Nature 545, 482–486.

Liu, Z.-Y., Li, X.-F., Jiang, T., Deng, Y.-Q., Ye, Q., Zhao, H., Yu, J.-Y., Qin, C.-F., 2016. Viral RNA switch mediates the dynamic control of flavivirus replicase recruitment by genome cyclization. Elife 5, e17636.

Long, F., Doyle, M., Fernandez, E., Miller, A.S., Klose, T., Sevvana, M., Bryan, A., Davidson, E., Doranz, B.J., Kuhn, R.J., Diamond, M.S., Crowe, J.E., Rossmann, M.G., 2019. Structural basis of a potent human monoclonal antibody against Zika virus targeting a quaternary epitope. Proc. Natl. Acad. Sci. Unit. States Am. 116, 1591.

Luan, B., Wang, H., Huynh, T., 2021. Enhanced binding of the N501Y-mutated SARS-CoV-2 spike protein to the human ACE2 receptor: insights from molecular dynamics simulations. FEBS (Fed. Eur. Biochem. Soc.) Lett. 595, 1454–1461.

Manangeeswaran, M., Ireland, D.D., Verthelyi, D., 2016. Zika (PRVABC59) infection is associated with T cell infiltration and neurodegeneration in CNS of immunocompetent neonatal C57Bl/6 mice. PLoS Pathog. 12, e1006004.

Miner Jonathan, J., Cao, B., Govero, J., Smith Amber, M., Fernandez, E., Cabrera Omar, H., Garber, C., Noll, M., Klein Robyn, S., Noguchi Kevin, K., Mysorekar Indira, U., Diamond Michael, S., 2016. Zika virus infection during pregnancy in mice causes placental damage and fetal demise. Cell 165, 1081–1091.

Mlakar, J., Korva, M., Tul, N., Popović, M., Poljšak-Prijatelj, M., Mraz, J., Kolenc, M., Resman Rus, K., Vesnaver Vipotnik, T., Fabjan Vodušek, V., Vizjak, A., Pižem, J., Petrovec, M., Avšič Županc, T., 2016. Zika virus associated with microcephaly. N. Engl. J. Med. 374, 951–958.

Musso, D., Ko, A.I., Baud, D., 2019. Zika virus infection — after the pandemic. N. Engl. J. Med. 381, 1444–1457.

Nem de Oliveira Souza, I., Frost, P.S., França, J.V., Nascimento-Viana, J.B., Neris, R.L.S., Freitas, L., Pinheiro, D.J.L.L., Nogueira, C.O., Neves, G., Chimelli, L., De Felice, F.G., Cavalheiro, É.A., Ferreira, S.T., Assunção-Miranda, I., Figueiredo, C.P., Da Poian, A.T., Clarke, J.R., 2018. Acute and chronic neurological consequences of early-life Zika virus infection in mice. Sci. Transl. Med. 10, eaar2749.

Nielsen-Saines, K., Brasil, P., Kerin, T., Vasconcelos, Z., Gabaglia, C.R., Damasceno, L., Pone, M., Abreu de Carvalho, L.M., Pone, S.M., Zin, A.A., Tsui, I., Salles, T.R.S., da Cunha, D.C., Costa, R.P., Malacarne, J., Reis, A.B., Hasue, R.H., Aizawa, C.Y.P., Genovesi, F.F., Einspieler, C., Marschik, P.B., Pereira, J.P., Gaw, S.L., Adachi, K., Cherry, J.D., Xu, Z., Cheng, G., Moreira, M.E., 2019. Delayed childhood neurodevelopment and neurosensory alterations in the second year of life in a prospective cohort of ZIKV-exposed children. Nat. Med. 25, 1213–1217.

Niu, X., Zhao, L., Qu, L., Yao, Z., Zhang, F., Yan, Q., Zhang, S., Liang, R., Chen, P., Luo, J., Xu, W., Lv, H., Liu, X., Lei, H., Yi, C., Li, P., Wang, Q., Wang, Y., Yu, L., Zhang, X., Bryan, L.A., Davidson, E., Doranz, jB., Feng, L., Pan, W., Zhang, F., Chen, L., 2019. Convalescent patient-derived monoclonal antibodies targeting different epitopes of E protein confer protection against Zika virus in a neonatal mouse model. Emerg. Microb. Infect. 8, 749–759.

Pierson, T.C., Diamond, M.S., 2018. The emergence of Zika virus and its new clinical syndromes. Nature 560, 573–581.

Pokidysheva, E., Zhang, Y., Battisti, A.J., Bator-Kelly, C.M., Chipman, P.R., Xiao, C., Gregorio, G.G., Hendrickson, W.A., Kuhn, R.J., Rossmann, M.G., 2006. Cryo-EM reconstruction of dengue virus in complex with the carbohydrate recognition domain of DC-SIGN. Cell 124, 485–493.

Rathore, A.P.S., Saron, W.A.A., Lim, T., Jahan, N., St John, A.L., 2019. Maternal immunity and antibodies to dengue virus promote infection and Zika virus–induced microcephaly in fetuses. Sci. Adv. 5, eaav3208.

Rey, F.A., 2003. Dengue virus envelope glycoprotein structure: new insight into its interactions during viral entry. Proc. Natl. Acad. Sci. Unit. States Am. 100, 6899.

Robbiani, D.F., Olsen, P.C., Costa, F., Wang, Q., Oliveira, T.Y., Nery Jr., N., Aromolaran, A., do Rosário, M.S., Sacramento, G.A., Cruz, J.S., Khouri, R., Wunder Jr., E.A., Mattos, A., de Paula Freitas, B., Sarno, M., Archanjo, G., Daltro, D., Carvalho, G.B.S., Pimentel, K., de Siqueira, I.C., de Almeida, J.R.M., Henriques, D.F., Lima, J.A., Vasconcelos, P.F.C., Schaefer-Babajew, D., Azzopardi, S.A., Bozzacco, L., Gazumyan, A., Belfort Jr., R., Alcântara, A.P., Carvalho, G., Moreira, A., Araujo, K., Reis, M.G., Keesler, R.I., Coffey, L.L., Tisoncik-Go, J., Gale Jr., M., Rajagopal, L., Adams Waldorf, K.M., Dudley, D.M., Simmons, H.A., Mejia, A., O'Connor, D.H., Steinbach, R.J., Haese, N., Smith, J., Lewis, A., Colgin, L., Roberts, V., Frias, A., Kelleher, M., Hirsch, A., Streblow, D.N., Rice, C.M., MacDonald, M.R., de Almeida, A.R.P., Van Rompay, K.K.A., Ko, A.I., Nussenzweig, M.C., 2019. Risk of Zika microcephaly correlates with features of maternal antibodies. J. Exp. Med. 216, 2302–2315.

Rossi, S.L., Tesh, R.B., Azar, S.R., Muruato, A.E., Hanley, K.A., Auguste, A.J., Langsjoen, R.M., Paessler, S., Vasilakis, N., Weaver, S.C., 2016. Characterization of a novel murine model to study Zika virus. The American Society of Tropical Medicine and Hygiene 94, 1362–1369.

Sapparapu, G., Fernandez, E., Kose, N., Bin, C., Fox, J.M., Bombardi, R.G., Zhao, H., Nelson, C.A., Bryan, A.L., Barnes, T., Davidson, E., Mysorekar, I.U., Fremont, D.H., Doranz, B.J., Diamond, M.S., Crowe, J.E., 2016. Neutralizing human antibodies prevent Zika virus replication and fetal disease in mice. Nature 540, 443–447.

Semple, B.D., Blomgren, K., Gimlin, K., Ferriero, D.M., Noble-Haeusslein, L.J., 2013. Brain development in rodents and humans: identifying benchmarks of maturation and vulnerability to injury across species. Prog. Neurobiol. 106–107, 1–16.

Shan, C., Xie, X., Muruato Antonio, E., Rossi Shannan, L., Roundy Christopher, M., Azar Sasha, R., Yang, Y., Tesh Robert, B., Bourne, N., Barrett Alan, D., Vasilakis, N., Weaver Scott, C., Shi, P.-Y., 2016. An infectious cDNA clone of Zika virus to study viral virulence, mosquito transmission, and antiviral inhibitors. Cell Host Microbe 19, 891–900.

Shao, Q., Herrlinger, S., Zhu, Y.-N., Yang, M., Goodfellow, F., Stice, S.L., Qi, X.-P., Brindley, M.A., Chen, J.-F., 2017. The African Zika virus MR-766 is more virulent and causes more severe brain damage than current Asian lineage and dengue virus. Development 144, 4114–4124.

Shioda, T., Levy, J.A., Cheng-Mayer, C., 1991. Macrophage and T cell-line tropisms of HIV-1 are determined by specific regions of the envelope gp!20 gene. Nature 349, 167–169.

Shioda, T., Levy, J.A., Cheng-Mayer, C., 1992. Small amino acid changes in the V3 hypervariable region of gp120 can affect the T-cell-line and macrophage tropism of human immunodeficiency virus type 1. Proc. Natl. Acad. Sci. Unit. States Am. 89, 9434.

Simonin, Y., Loustalot, F., Desmetz, C., Foulongne, V., Constant, O., Fournier-Wirth, C., Leon, F., Molès, J.-P., Goubaud, A., Lemaitre, J.-M., Maquart, M., Leparc-Goffart, I., Briant, L., Nagot, N., Van de Perre, P., Salinas, S., 2016. Zika virus strains potentially display different infectious profiles in human neural cells. EBioMedicine 12, 161–169.

Udenze, D., Trus, I., Berube, N., Gerdts, V., Karniychuk, U., 2019. The African strain of Zika virus causes more severe in utero infection than Asian strain in a porcine fetal transmission model. Emerg. Microb. Infect. 8, 1098–1107.

Vasile, F., Dossi, E., Rouach, N., 2017. Human astrocytes: structure and functions in the healthy brain. Brain Struct. Funct. 222, 2017–2029.

Wang, Q., Yang, H., Liu, X., Dai, L., Ma, T., Qi, J., Wong, G., Peng, R., Liu, S., Li, J., Li, S., Song, J., Liu, J., He, J., Yuan, H., Xiong, Y., Liao, Y., Li, J., Yang, J., Tong, Z., Griffin, B.D., Bi, Y., Liang, M., Xu, X., Qin, C., Cheng, G., Zhang, X., Wang, P., Qiu, X., Kobinger, G., Shi, Y., Yan, J., Gao, G.F., 2016. Molecular determinants of human neutralizing antibodies isolated from a patient infected with Zika virus. Sci. Transl. Med. 8, 369ra179.

Xia, H., Luo, H., Shan, C., Muruato, A.E., Nunes, B.T.D., Medeiros, D.B.A., Zou, J., Xie, X., Giraldo, M.I., Vasconcelos, P.F.C., Weaver, S.C., Wang, T., Rajsbaum, R., Shi, P.-Y., 2018. An evolutionary NS1 mutation enhances Zika virus evasion of host interferon induction. Nat. Commun. 9, 414.

Yockey, L.J., Varela, L., Rakib, T., Khoury-Hanold, W., Fink, S.L., Stutz, B., Szigeti-Buck, K., Van den Pol, A., Lindenbach, B.D., Horvath, T.L., Iwasaki, A., 2016. Vaginal exposure to Zika virus during pregnancy leads to fetal brain infection. Cell 166, 1247–1256 e1244.

Yuan, L., Huang, X.-Y., Liu, Z.-Y., Zhang, F., Zhu, X.-L., Yu, J.-Y., Ji, X., Xu, Y.-P., Li, G., Li, C., Wang, H.-J., Deng, Y.-Q., Wu, M., Cheng, M.-L., Ye, Q., Xie, D.-Y., Li, X.-F., Wang, X., Shi, W., Hu, B., Shi, P.-Y., Xu, Z., Qin, C.-F., 2017. A single mutation in the prM protein of Zika virus contributes to fetal microcephaly. Science 358, 933.

Zhang, F., Wang, H.-J., Wang, Q., Liu, Z.-Y., Yuan, L., Huang, X.-Y., Li, G., Ye, Q., Yang, H., Shi, L., Deng, Y.-Q., Qin, C.-F., Xu, Z., 2017. American strain of Zika virus causes more severe microcephaly than an old Asian strain in neonatal mice. EBioMedicine 25, 95–105.

Zhou, H.Y., Ji, C.Y., Fan, H., Han, N., Li, X.F., Wu, A., Qin, C.F., 2021. Convergent evolution of SARS-CoV-2 in human and animals. Protein Cell 12, 832–835.